Journal of Pathology
J Pathol October 2024; **264:** 212–227
Published online 23 August 2024 in Wiley Online Library
(wileyonlinelibrary.com) DOI: 10.1002/path.6339

ORIGINAL ARTICLE

Single-cell transcriptomics identifies aberrant glomerular angiogenic signalling in the early stages of WT1 kidney disease

Jennifer C Chandler[1,2], Daniyal J Jafree[1,2,3], Saif Malik[1,2], Gideon Pomeranz[1,2], Mary Ball[1,2], Maria Kolatsi-Joannou[1,2], Alice Piapi[1], William J Mason[1,2], Andrew V Benest[4], David O Bates[4,5], Aleksandra Letunovska[1,6], Reem Al-Saadi[1,6], Marion Rabant[7], Olivia Boyer[8], Kathy Pritchard-Jones[1], Paul J Winyard[1,2], Andrew S Mason[9], Adrian S Woolf[10,11], Aoife M Waters[1] and David A Long[1,2*]

[1] *Developmental Biology and Cancer Research and Teaching Department, University College London Great Ormond Street Institute of Child Health, London, UK*
[2] *UCL Centre for Kidney and Bladder Health, London, UK*
[3] *UCL MB/PhD Programme, Faculty of Medical Sciences, University College London, London, UK*
[4] *Endothelial Quiescence Group and Tumour and Vascular Biology Laboratories, Division of Cancer and Stem Cells, Centre for Cancer Sciences, School of Medicine, Biodiscovery Institute, University of Nottingham, Nottingham, UK*
[5] *Pan-African Cancer Research Institute, University of Pretoria, Hatfield, South Africa*
[6] *Department of Histopathology, Great Ormond Street Hospital for Children NHS Foundation Trust, London, UK*
[7] *Pathology department, Hôpital Universitaire Necker-Enfants Malades, Institut Imagine, Université Paris Cité, Paris, France*
[8] *APHP, Service de Néphrologie Pédiatrique, Hôpital Universitaire Necker-Enfants Malades, Institut Imagine, Université Paris Cité, Paris, France*
[9] *Department of Biology and York Biomedical Research Institute, University of York, UK*
[10] *Faculty of Biology, Medicine and Health, University of Manchester, Manchester, UK*
[11] *Royal Manchester Children's Hospital, Manchester University NHS Foundation Trust, Manchester Academic Health Science Centre, Manchester, UK*

**Correspondence to: DA Long, Developmental Biology and Cancer Research and Teaching Department, UCL Great Ormond Street Institute of Child Health, London WC1N 1EH, UK. E-mail: d.long@ucl.ac.uk*

Abstract

WT1 **encodes a podocyte transcription factor whose variants can cause an untreatable glomerular disease in early childhood. Although WT1 regulates many podocyte genes, it is poorly understood which of them are initiators in disease and how they subsequently influence other cell-types in the glomerulus. We hypothesised that this could be resolved using single-cell RNA sequencing (scRNA-seq) and ligand–receptor analysis to profile glomerular cell–cell communication during the early stages of disease in mice harbouring an orthologous human mutation in WT1 (*$Wt1^{R394W/+}$*). Podocytes were the most dysregulated cell-type in the early stages of *$Wt1^{R394W/+}$* disease, with disrupted angiogenic signalling between podocytes and the endothelium, including the significant downregulation of transcripts for the vascular factors Vegfa and Nrp1. These signalling changes preceded glomerular endothelial cell loss in advancing disease, a feature also observed in biopsy samples from human WT1 glomerulopathies. Addition of conditioned medium from murine *$Wt1^{R394W/+}$* primary podocytes to wild-type glomerular endothelial cells resulted in impaired endothelial looping and reduced vascular complexity. Despite the loss of key angiogenic molecules in *$Wt1^{R394W/+}$* podocytes, the pro-vascular molecule adrenomedullin was upregulated in *$Wt1^{R394W/+}$* podocytes and plasma and its further administration was able to rescue the impaired looping observed when glomerular endothelium was exposed to *$Wt1^{R394W/+}$* podocyte medium. In comparative analyses, adrenomedullin upregulation was part of a common injury signature across multiple murine and human glomerular disease datasets, whilst other gene changes were unique to WT1 disease. Collectively, our study describes a novel role for altered angiogenic signalling in the initiation of WT1 glomerulopathy. We also identify adrenomedullin as a proangiogenic factor, which despite being upregulated in early injury, offers an insufficient protective response due to the wider milieu of dampened vascular signalling that results in endothelial cell loss in later disease.**

Keywords: adrenomedullin; childhood glomerular disease; glomerular endothelium; neuropilin-1; podocyte; single-cell transcriptomics; WT1 glomerulopathy; vascular endothelial growth factor-A

Received 21 March 2024; Revised 17 June 2024; Accepted 28 June 2024

No conflicts of interest were declared.

Introduction

Mutations in the podocyte transcription factor *Wilms tumour 1* (*WT1*) account for around 15% of genetically diagnosed congenital glomerular diseases [1]. There are no specific drug treatments for WT1 glomerulopathy, with cases being unresponsive to glucocorticoids and second-line immunosuppressive drugs [1,2]. WT1 adopts both activation and repressive functions [3] and directly regulates approximately half of all podocyte-specific genes [4,5], at least 18 of which have known variants resulting in congenital glomerulopathies [5]. Genomic investigation into pairwise interactions between WT1 and its genetic targets [4–6] has advanced our knowledge of the WT1-regulated podocyte transcriptome, but we still lack an integrated understanding of how WT1 initiates multicellular glomerular decline and how this can be treated.

One approach to explore glomerular pathophysiology is to use single-cell RNA sequencing (scRNA-seq), a technique which has characterised the multicellular transcriptional landscape of glomerular health [7] and disease [8–10]. Most studies to date have focused on experimentally induced, adult pathologies [8–10], rather than models replicating genetic mutations observed in the paediatric population. Therefore, we performed scRNA-seq on glomeruli from a clinically relevant murine model of WT1 childhood-onset glomerulopathy ($Wt1^{R394W/+}$) [11]. These mice carry a heterozygous point mutation in *WT1*, resulting in the substitution of a tryptophan for arginine at codon 394 in the DNA-binding, third zinc finger (*WT1* c.1180C > T; p.R394W). This mutation is orthologous to a paediatric hotspot mutation, accounting for around 30% of all identified *WT1* mutations [12] and the most common mutation found in Denys–Drash syndrome [13] (DDS, OMIM #194080), characterised by early onset steroid-resistant nephrotic syndrome (SRNS) and diffuse mesangial sclerosis (DMS) [12].

Using the $Wt1^{R394W/+}$ mouse, we generated a glomerular transcriptomic dataset at single-cell resolution, exploring the early stages of an early-onset childhood disease. Using cell-specific differential expression and ligand-receptor interaction analyses, we reveal early transcriptional characteristics of mutant podocytes, including disrupted angiogenic signalling, with the loss of key vascular factors, preceding glomerular capillary loss. Accordingly, tube formation was impaired in glomerular endothelial cells (GECs) exposed to conditioned medium from $Wt1^{R394W/+}$ podocytes. Despite this overall anti-angiogenic environment in *Wt1* glomerular disease, we found an upregulation of the vascular peptide adrenomedullin in $Wt1^{R394W/+}$ podocytes and plasma. Further administration of adrenomedullin reversed the impairment of GEC tube formation induced by $Wt1^{R394W/+}$ podocyte medium, suggesting an insufficient protective response. Wider transcriptomic analysis found adrenomedullin as part of a common glomerular-injury signature across multiple murine and human glomerular disease datasets.

Materials and methods

Experimental animals

Animal procedures were approved by the UK Home Office. Male C57BL/6 mice heterozygous for *Wt1 c.1800 C > T* p. R394W [11] were backcrossed with MF1 females (Charles River, Margate, UK) for two generations [11]; second-generation male offspring ($Wt1^{R394W/+}$) were used for all subsequent analysis. Histological and biochemical assessment is outlined in Supplementary materials and methods.

Glomerular isolation, single-cell processing and analysis

Representative individuals ($n = 2$) for $Wt1^{+/+}$ and $Wt1^{R394W/+}$ mice were used for scRNA-seq. Glomeruli were isolated as described [8,14] with some adaptations to maximise podocyte yield (see Supplementary materials and methods). Glomerular single-cell suspensions from $Wt1^{+/+}$ and $Wt1^{R394W/+}$ mice were processed in parallel using the Chromium Next GEM Single Cell 3' Reagent Kits version 3.1 (Dual Index) kit (10x Genomics, Pleasanton, CA, USA) following the manufacturer's instructions. Cell-type clusters were identified using canonical markers of glomerular cells and informed by published murine scRNA-seq studies [8,15–17]. WT1 motif analysis was performed using CiiiDER [18] and inference of glomerular intercellular communication was determined using NICHES [18]. Detailed protocols are in the Supplementary materials and methods.

Cross-disease comparison of podocyte differential gene expression

To compare podocytes in $Wt1^{R394W/+}$ glomerulopathy with other models of early glomerular disease, publicly accessible scRNA-seq data from Dynabead isolated glomeruli were used [8]. Conserved murine genes (found in all four analysed murine scRNA-seq datasets) underwent targeted screening for similar dysregulation (fold-change>0.25 and $p < 0.05$) in human microarray glomerular datasets in the Nephroseq database nephroseq.org.

Immunofluorescence

Immunofluorescence staining was performed on murine tissue using antibodies against WT1 (1:100, ab89901, Abcam, Cambridge, UK), F4/80 (MCA497G, Bio-Rad, Oxford, UK) and CD31 (1:400, MA3105, ThermoFisher, Waltham, MA, USA) and on human tissue using an anti-CD31 antibody (1: 200, ab76533, Abcam). Analysis was conducted in FIJI [19] as outlined in Supplementary materials and methods.

Primary podocyte harvest, RT-qPCR and tube formation assays

For primary podocyte harvest, glomeruli were isolated from $Wt1^{+/+}$ and $Wt1^{R394W/+}$ mice at 4 weeks of age as

described [20]; see Supplementary materials and methods for details. Podocyte RNA was extracted (74136, Qiagen, Manchester, UK) and cDNA prepared using the gDNA Clear cDNA Synthesis Kit (172-5,035, Bio-Rad, Oxford, UK). Reverse transcription-quantitative polymerase chain reaction (RT-qPCR) was performed in duplicate using qPCRBIO SyGreen Mix Lo-ROX (PB20.11–05, PCRBioSystems, London, UK) with specific primers for *Vegfa* and *Nrp1* standardised to *Gapdh*. Tube formation assays were conducted with medium conditioned by primary podocytes isolated from $Wt1^{+/+}$ and $Wt1^{R394W/+}$ mice at 4 weeks of age, which were added to wild-type primary murine GECs (C57-6014G, Cell Biologics, Chicago, IL, USA) and analysed using FastTrack AI (MetaVi Labs, Austin, TX, USA); see Supplementary materials and methods for details.

Statistical methods

Differences between $Wt1^{+/+}$ and $Wt1^{R394W/+}$ groups were analysed using Prism (GraphPad Inc, Boston, MA, USA). Normality was assessed using a Shapiro–Wilk test, and if necessary, data converted to a log scale before analysis using relevant parametric statistical tests. Significance was accepted at $p < 0.05$ and data in graphs are presented as mean ± SD.

Results

Time course of disease progression in $Wt1^{R394W/+}$ mice

The glomerulus is a specialised multicellular niche (Figure 1A) that becomes structurally and functionally compromised in WT1 glomerulopathy. Prior work has shown that $Wt1^{R394W/+}$ kidneys appear histologically normal at birth and 3 weeks of age, with proteinuria present by 8 weeks [11]. To further understand the relationship between renal structure and function, we compared histology with urinary albumin/creatinine ratio (ACR) and blood urea nitrogen (BUN) levels from 4 weeks of age. At 4 weeks of age, in the absence of any overt histological pathology of DMS (Figure 1B), urinary ACR was significantly elevated ($\log_{10}$ ACR 3.96 ± 0.08 µg/mg; $p < 0.0001$) in $Wt1^{R394W/+}$ mice compared with $Wt1^{+/+}$ wild-type littermates (1.91 ± 0.05 µg/mg; Figure 1C), indicating glomerular filtration barrier impairment. In contrast, BUN levels were similar between $Wt1^{+/+}$ (45.97 ± 1.65 mg/dl) and $Wt1^{R394W/+}$ mice (50.74 ± 2.60 mg/dl) (Figure 1D). By 8 weeks of age, ACR remained significantly elevated in $Wt1^{R394W/+}$ mice (3.48 ± 0.15 µg/mg) compared with $Wt1^{+/+}$ animals (2.21 ± 0.12 µg/mg; $p < 0.0001$, Figure 1C), and histologically, glomeruli showed mesangial matrix expansion, disorganised vasculature and tuft fibrosis, pathological features of DMS (Figure 1B). BUN levels were significantly increased by 8 weeks ($Wt1^{R394W/+}$, 62.07 ± 2.54 mg/dl versus $Wt1^{+/+}$ littermates, 48.45 ± 1.81 mg/dl; $p = 0.0006$, Figure 1D). Together this suggests that 4 weeks represents an early disease timepoint in $Wt1^{R394W/+}$ mice, when disease is clinically manifested, prior to widespread glomerular scaring and deterioration of renal excretory function.

Generation of a glomerular single-cell transcriptomic dataset to characterise the onset of WT1 glomerulopathy

To identify initiators of disease progression, we performed scRNA-seq on glomeruli isolated by Dynabead perfusion (supplementary material, Figure S1A) from biochemically representative 4-week-old $Wt1^{+/+}$ and $Wt1^{R394W/+}$ mice (supplementary material, Figure S1B,C). Single-cell suspensions were generated using a protocol [8,14] optimised to maximise podocyte viability and yield. Live cells were individually isolated and sequenced to generate an aggregated atlas of 6,846 cells. Eleven transcriptionally distinct cell identities (Figure 1E) were defined by canonical markers [8,15–17], including two $Wt1^{+}$ $Nphs2^{+}$ podocyte clusters, $Emcn^{+}$ $Ehd3^{+}$ GECs, Ptn^{+} $Pdgfrb^{+}$ mesangium, $Sox17^{+}$ arterial endothelium, including $Plvap^{+}$ efferent arterioles and $Edn1^{+}$ afferent arterioles, $Acta2^{+}$ $Myh11^{+}$ smooth muscle and $Pax8^{+}$ $Cldn1^{+}$ parietal epithelial cells (PECs). Leukocyte subsets were identified, including a $Lyz2^{+}$ myeloid cluster, $Cd79a^{+}$ $Igkc^{+}$ B lymphocytes and $Cd3^{+}$ $Trbc2^{+}$ T lymphocytes (supplementary material, Figure S1D).

We confirmed assigned genotypes, demonstrating that the $C > T$ mutated allele was expressed as an average of 39% of total *Wt1* coverage in $Wt1^{R394W/+}$ mice (Figure 1F); in line with the original description of this model [11]. We allocated cells according to genotype within each cluster (Figure 1G and supplementary material, Figure S1E), revealing cells from both $Wt1^{+/+}$ and $Wt1^{R394W/+}$ mice in all glomerular cell-type clusters in similar proportions (supplementary material, Figure S1F). However, podocytes from $Wt1^{+/+}$ and $Wt1^{R394W/+}$ glomeruli resolved into distinct clusters in two-dimensional space, each corresponding to genotype (Figure 1E and supplementary material, Figure S1E,F).

Dysregulation of the podocyte transcriptome dominates early WT1 glomerulopathy

To examine cell-type specific changes associated with early WT1 glomerulopathy, we identified differentially expressed genes (DEGs) in podocytes, GECs, the mesangium and PECs (Figure 2A). Of the 3,710 captured genes in podocytes, 268 genes (7.22%) were significantly [$\log_2$ fold-change ($\log_2$FC) of ≥0.25 and adjusted $p < 0.05$] downregulated and 198 upregulated (5.34%) in $Wt1^{R394W/+}$ mice compared with $Wt1^{+/+}$ (Figure 2A). Conversely in GECs, 25/719 (3.48%) genes were downregulated, and 33/719 (4.5%) genes were upregulated. Comparatively low numbers of DEGs were observed in mesangial cells (12 genes; 1.76% downregulated and 25 genes; 3.66% upregulated) and PECs (6 genes; 1.54% upregulated) (Figure 2A and

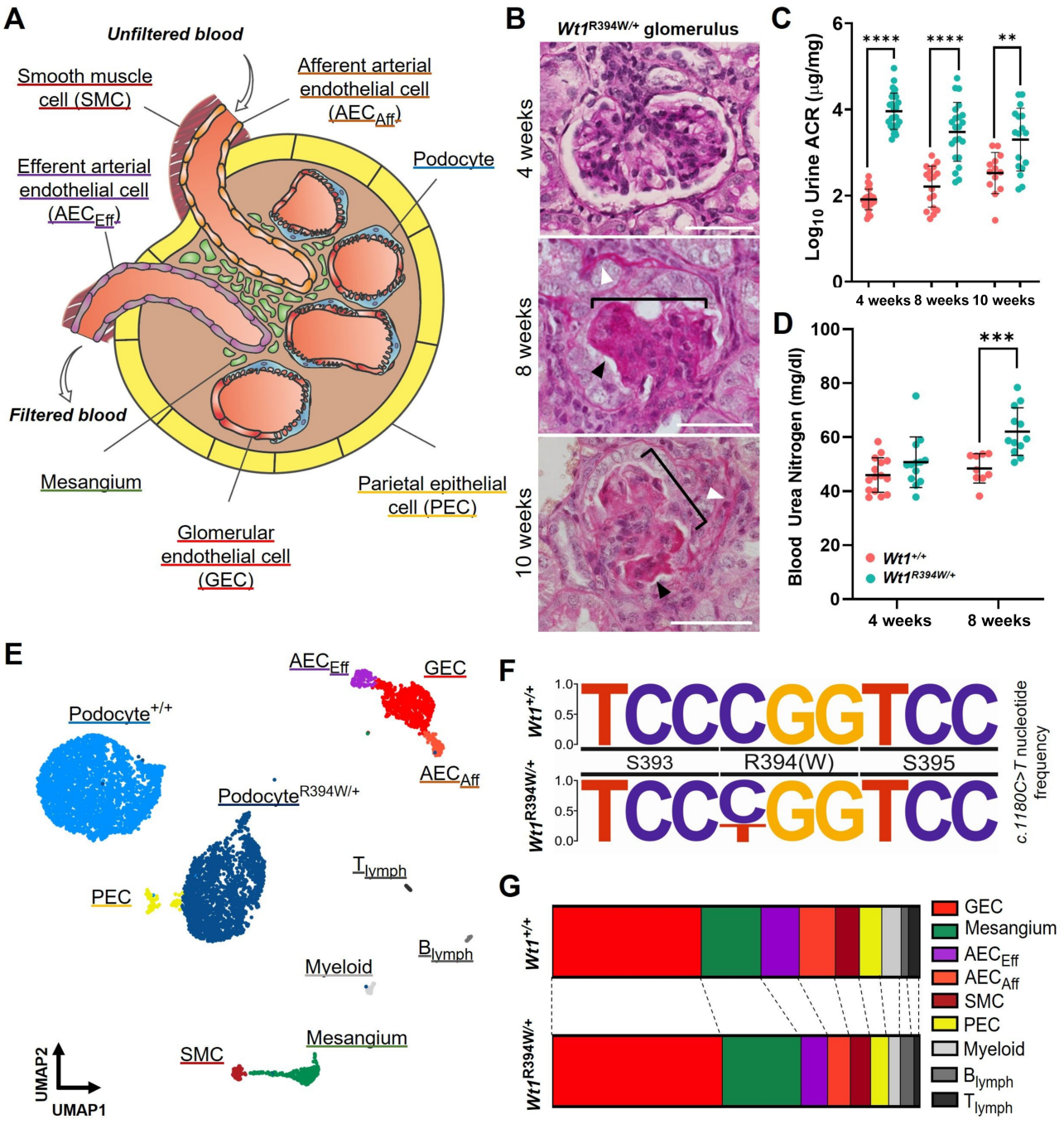

Figure 1. Defining early disease in *Wt1*$^{R394W/+}$ mice to generate a glomerular single-cell dataset for WT1 glomerulopathy. (A) The glomerular niche, composed of multiple specialised cell-types, which together orchestrate plasma filtration, removing toxic waste products for urinary excretion. (B) Glomeruli from *Wt1*$^{R394W/+}$ mutant kidneys show minimal scarring in early disease at 4 weeks of age, but by 8 weeks, glomeruli show defined features of diffuse mesangial sclerosis, seen as global expansion and scarring of mesangial matrix (black arrowhead), disorganised vasculature (white arrowhead) with shrinking and sclerosis of glomerular tuft (bracketed), these histological features are also seen at 10 weeks; scale bars: 50 µm. (C) Elevated albumin/creatinine ratio (ACR), indicative of early glomerular damage, is present in *Wt1*$^{R394W/+}$ mutant mice (turquoise) from 4 weeks of age, with significantly elevated $\log_{10}$ ACR compared with *Wt1*$^{+/+}$ littermates (pink) (*t*-test at 4 weeks; $p < 0.0001$; $n = 25, 28$; lines represent mean ± SD). (D) Blood urea nitrogen, indicative of renal deterioration, is elevated in *Wt1*$^{R394W/+}$ mice by 8 weeks of age (*t*-test; $p = 0.0006$, $n = 9, 12$; lines represent mean ± SD). (E) UMAP clustering of sequenced glomerular cells from *Wt1*$^{+/+}$ and *Wt1*$^{R394W/+}$ mice. A total of 6,846 cell-types resolved into 11 transcriptionally distinct cell clusters, of which only podocytes show two distinct clusters based on genotype. (F) Plot of *Wt1 c.1800 C > T* p. R394W substitution frequency in *Wt1*$^{R394W/+}$ mice, showing mutant T allele is at a lower frequency than the wildtype C, at an average of 39% presented. (G) Plots showing the proportions of each cell-type within each genotype, all non-podocyte cell-types are well represented across both *Wt1*$^{+/+}$ and *Wt1*$^{R394W/+}$.

supplementary material, Table S1). To assess whether podocyte transcriptional changes were caused directly by the aberrant binding of mutant WT1, we used CiiiDER [21] to predict the presence of WT1 binding motifs. We found 125 (46.64%) of the podocyte genes downregulated and 107 (54.04%) of those upregulated contained a predicted WT1 regulatory element within 1 kbp downstream and 500 base-pairs upstream [5] of

the transcriptional start site. This fits with previous reports that around half of podocyte-specific genes are direct targets of WT1 [4]. We compared our DEGs with those reported by Ratelade *et al* [22], who conducted bulk sequencing of glomeruli isolated from *Wt1*$^{R394W/+}$ FVB mutant mice, with minimal albuminuria. Of the

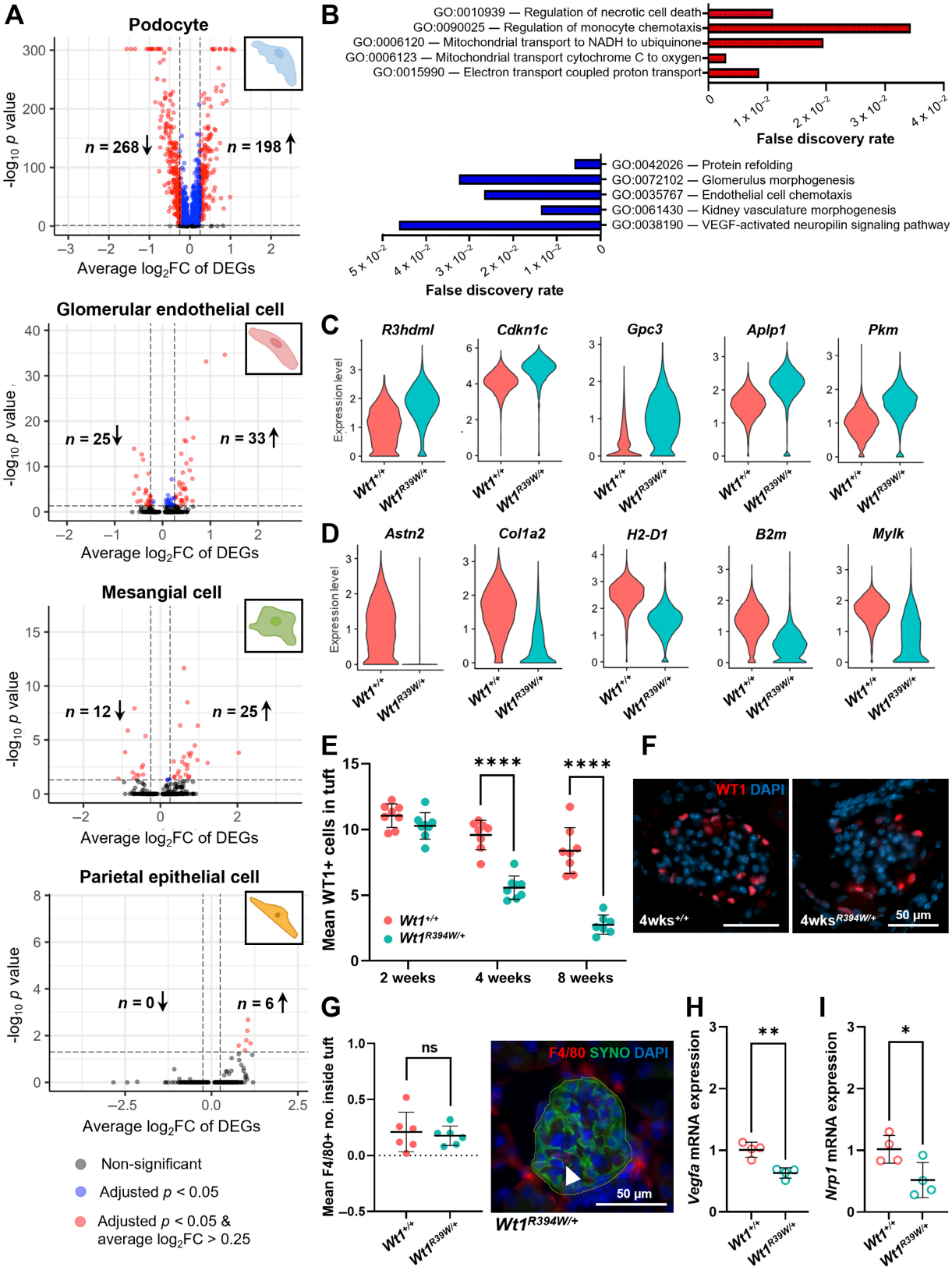

Figure 2 Legend on next page.

38 downregulated genes described by Ratelade *et al*, 15 were also present in our DEG lists in podocytes (*Col1a2*, *Ntrk3*, *Sulf1*, *Med24*, *Cd59a*, *Mgat4a*, *Fxyd6*, *Plxdc2*, *Cdon*, *Abr*, *Dock5*, *Dusp15*, *Aifm3*, *Pcsk6*, *Scel*), with *Cd59a*, *Sulf1* also downregulated in PECs. Of the 25 upregulated genes, six were present in our dataset, five of which were found in podocytes (*Cald1*, *Cyp26a1*, *Pstpip2*, *Ptgds*, *Reep1*) and one in GECs (*Mxra7*).

To identify the functional roles of DEGs in $Wt1^{R394W/+}$ podocytes, we conducted gene ontology (GO) analysis (Figure 2B). The top upregulated pathways in podocytes indicated metabolic disturbance and cell death. The latter contrasts with the proposed function of several of the top five upregulated genes in $Wt1^{R394W/+}$ podocytes (Figure 2C and supplementary material, Table S1), which adopt a protective response in glomerular injury. These include the podocyte-expressed peptidase inhibitor *R3hdml* ($\log_2$FC = 1.09) and pyruvate kinase (*Pkm*, $\log_2$FC = 0.87), the respective overexpression of which ameliorates TGF-β-induced apoptosis [23] and protects against mitochondrial dysfunction in murine diabetic nephropathy (DN) [24]. Similarly, p57 (*Cdkn1c*, $\log_2$FC = 1.04), the loss of which is associated with proliferation in animal models of podocyte injury [25,26] and patients with proliferative glomerular disease [27,28], is upregulated in $Wt1^{R394W/+}$ podocytes, a feature shown to be associated with reduced proliferation rates [25].

Of the downregulated genes in $Wt1^{R394W/+}$ podocytes, three of the top five associated GO pathways reflected dampened angiogenesis (Figure 2B). The top five downregulated transcripts included collagen α2(I) (*Col1a2*, $\log_2$FC = −1.45) and myosin light chain kinase (*Mylk*, $\log_2$FC = −1.02). The loss of *Col1a2*, present in the glomerular extracellular matrix of healthy mice [29], is associated with sclerotic mesangial matrix accumulation, a hallmark of DMS [30] and *Mylk* is involved in stress fibre and focal adhesion formation [31], critical for podocyte architecture. Reduced β2-microglobulin (*B2m*, $\log_2$FC = −1.07) has not been described, but is overexpressed in patients with glomerulonephritis [32] and elevated serum levels are associated with disease severity in DN [33]. Astrotactin-2 (*Astn2*, $\log_2$FC = −1.56) is a risk factor locus associated with reduced glomerular filtration rate [34] (Figure 2D).

To further examine the upregulation of pathways of '*cell-death*', we assessed podocyte ($WT1^+$) cell number through disease progression, finding fewer $WT1^+$ podocyte cells at 4 weeks in $Wt1^{R394W/+}$ mice (9.58 ± 0.40 cells/glomerular tuft in $Wt1^{+/+}$ mice versus 5.57 ± 0.31 in $Wt1^{R394W/+}$; $p < 0.0001$, Figure 2E,F), a finding exacerbated by 8 weeks ($Wt1^{+/+}$, 8.38 ± 0.62 versus $Wt1^{R394W/+}$, 2.75 ± 0.28; $p < 0.0001$), but undetectable in 2-week-old mice (11.04 ± 0.32 and 10.27 ± 0.35 cells/glomerular tuft respectively). To verify our clustering data showing equal proportions of immune cells in $Wt1^{+/+}$ and $Wt1^{R394W/+}$ glomeruli (Figure 1G and supplementary material, Figure S1F) considering the upregulation of GO:0090025 – *regulation of monocyte chemotaxis* in $Wt1^{R394W/+}$ podocytes (Figure 2B), we examined monocyte infiltration *in situ* at 4 weeks, through myeloid marker $F4/80^+$. This found similar intraglomerular $F4/80^+$ cell numbers in $Wt1^{+/+}$ (0.21 ± 0.07 cells) and $Wt1^{R394W/+}$ mice (0.18 ± 0.04 cells; $p = 0.6864$; Figure 2G), which was also the case for extraglomerular $F4/80^+$ cell counts (supplementary material, Figure S1G). Regarding the pronounced dampening of angiogenic signalling, RT-qPCR of primary podocytes isolated at 4 weeks of age (supplementary material, Figure S2A,B) demonstrated downregulation of both vascular endothelial growth factor A [*Vegfa* ($Wt1^{+/+}$ 1.01 ± 0.06 versus $Wt1^{R394W/+}$ 0.63 ± 0.04); $p = 0.0021$ Figure 2H] and Neuropilin-1 (*Nrp1*, $Wt1^{+/+}$, 1.02 ± 0.11 versus $Wt1^{R394W/+}$ 0.52 ± 0.14; $p = 0.033$ Figure 2I) in $Wt1^{R394W/+}$ podocytes. This describes a down-regulation that persists *ex vivo*, outside of the native environment, in accord with the presence of predicted WT1 binding motifs (supplementary material, Table S1) and previous evidence that WT1 directly regulates *VEGFA* [5,35].

Characterisation of the glomerular cell–cell communication landscape identifies defective angiogenic signalling in early WT1 glomerulopathy, associated with endothelial cell loss

Next, we focused on how $Wt1^{R394W/+}$ podocytes might impact other glomerular cells by conducting ligand-receptor analysis using the NICHES package [18], predicting paracrine and physical interactions at single-cell resolution. Partitioning our scRNA-seq atlas by genotype, we conducted unsupervised clustering from the NICHES output to generate interaction maps of the intercellular communication landscape in $Wt1^{+/+}$ and $Wt1^{R394W/+}$ glomeruli. Distinct interaction clusters between podocytes and GECs (Figure 3A), mesangial

Figure 2. Cell-specific differential expression analyses in the glomerulus shows podocytes as the most affected cell in early WT1 glomerulopathy. (A) Volcano plots showing differentially expressed genes (DEGs) in $Wt1^{R394W/+}$ podocytes (significant hits show average $\log_2$ fold change (FC) >0.25 and adjusted *p* value <0.05) for podocytes, glomerular endothelial cells, mesangial cells and parietal epithelial cells, showing podocytes as having the highest number and proportion of DEGs. (B) Gene ontology (GO) pathway analyses of podocyte DEGs, showing the top five upregulated (red) and downregulated (blue) pathways. (C) Violin plots of the top five upregulated and (D) downregulated genes in $Wt1^{R394W/+}$ podocytes. (E, F) Podocyte ($WT1^+$) cell counts in glomeruli at 2, 4 and 8 weeks of age show a significant decline in podocyte number from 4 weeks of age (*t*-test; $p < 0.0001$, $n = 8$ mice per group), further reduced by 8 weeks (*t*-test; $p < 0.0001$, $n = 8$ mice per group). (G) Myeloid ($F4/80^+$) cell counts within the tuft of 4-week-old glomeruli show no difference between $Wt1^{+/+}$ and $Wt1^{R394W/+}$ mice (*t*-test; $p = 0.6864$, $n = 6$ mice per group). (H) Reverse transcription-quantitative polymerase chain reaction (RT-qPCR) quantified transcript levels of vascular endothelial growth factor A (*Vegfa*) in $Wt1^{+/+}$ and $Wt1^{R394W/+}$ primary podocytes isolated from mice at 4 weeks of age show a significant decline in *Vegfa* in $Wt1^{R394W/+}$ podocytes (*t*-test; $p = 0.0021$; $n = 4$ mice per group). (I) RT-qPCR quantified transcript levels of neuropilin-1 (*Nrp1*) in $Wt1^{+/+}$ and $Wt1^{R394W/+}$ primary podocytes isolated from mice at 4 weeks of age show a significant decline in *Nrp1* in $Wt1^{R394W/+}$ podocytes (*t*-test; $p = 0.0333$; $n = 4$ mice per group).

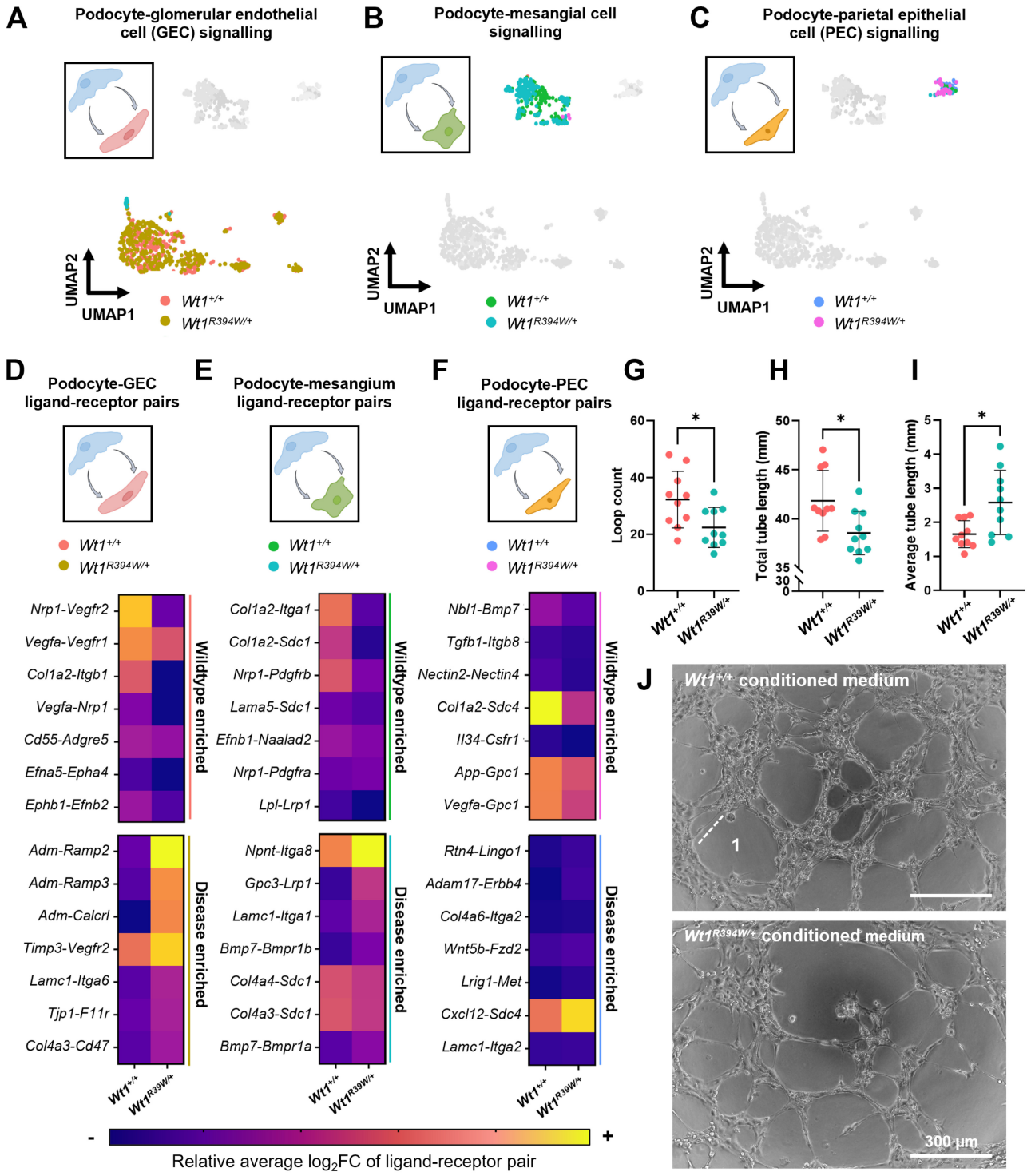

Figure 3. Altered intercellular signalling between $Wt1^{R394W/+}$ podocytes and glomerular endothelial, mesangial and parietal epithelial cells and associated disruption to endothelial angiogenesis. Ligand–receptor interaction analysis was performed using the NICHES package [18] to infer intercellular communication between podocytes and (A) glomerular endothelial cells (GECs), (B) mesangial cells and (C) parietal epithelial cells (PECs). A UMAP enabled visualisation of pairwise interactions between cell-types in two-dimensional space, with the following colouring: orange ($Wt1^{+/+}$ podocytes – $Wt1^{+/+}$ GEC), yellow ($Wt1^{R394W/+}$ podocytes – $Wt1^{R394W/+}$ GEC), green ($Wt1^{+/+}$ podocytes – $Wt1^{+/+}$ mesangium), light blue ($Wt1^{R394W/+}$ podocytes – $Wt1^{R394W/+}$ mesangium), dark blue ($Wt1^{+/+}$ podocytes – $Wt1^{+/+}$ PEC), magenta ($Wt1^{R394W/+}$ podocytes – $Wt1^{R394W/+}$ PEC). (D–F) Heatmaps showing average $\log_2$ fold change (FC) of the top seven enriched ligand–receptor interactions (by lowest adjusted p value) in $Wt1^{+/+}$ and $Wt1^{R394W/+}$ glomeruli. (G–I) Tube formation in murine GECs cultured in media conditioned by primary podocytes isolated from $Wt1^{+/+}$ and $Wt1^{R394W/+}$ mice at 4 weeks of age. $Wt1^{R394W/+}$ conditioned medium resulted in (G) fewer loops (t-test; $p = 0.0141$, $n = 10$ mice per group), (H) a reduction in total tube length (t-test; $p = 0.0141$, $n = 10$ mice per group) and (I) increased individual tube length (t-test; $p = 0.0104$, $n = 10$ mice per group). (J) Representative images of endothelial tube formation in $Wt1^{+/+}$ and $Wt1^{R394W/+}$ podocyte conditioned media, a single loop (1) and individual tube length (dashed line) are indicated.

cells (Figure 3B) and PECs (Figure 3C) were apparent, with no genotype-specific interactions observed.

We examined if the relative strength, defined as the most statistically significant interactions by NICHES, were altered (defined by log_2FC) between $Wt1^{+/+}$ and $Wt1^{R394W/+}$ glomeruli. Between podocytes and GECs (Figure 3D), angiogenic signals involved in the fine-tuning of trans-cellular (between cell) VEGF signalling [36], including *Nrp1-Vegfr2*, *Vegfa-Vegfr1* and *Vegfa-Nrp1*, were enriched in healthy glomeruli (Figure 3D). However, these interactions were lost in $Wt1^{R394W/+}$ glomeruli, reflecting the reduction of *Nrp1* and *Vegfa* in mutant podocytes, as neither *Vegfr1* nor *Vegfr2* were differentially expressed in $Wt1^{R394W/+}$ GECs, with *Nrp1* expression showing a significant increase (supplementary material, Table S1). In contrast, podocyte to endothelial interactions enriched in $Wt1^{R394W/+}$ mice involved adrenomedullin (*Adm*) and its receptors (*Adm-Ramp2*, *Adm-Ramp3* and *Adm-Calcrl*), implicated in angiogenesis [37] and vascular barrier permeability [38]. *Adm* was detected in the top 20 upregulated (supplementary material, Table S1) genes in $Wt1^{R394W/+}$ podocytes and its upregulation has been reported in experimental models of podocyte injury [39–41]. Several glomerular interactions involving podocyte *Col1a2* were altered in disease, with connections between mesangial integrin α1 (*Col1a2–Itga1*) and syndecan-1 (*Col1a2–Scd1*) and PEC syndecan-4 (*Col1a2–Sdc4*) lost in $Wt1^{R394W/+}$ mice (Figure 3E,F). Podocyte–mesangial interactions enriched in disease involved nephronectin (*Npnt–Itga8*), glypican-3 (*Gpc3–Lrp1*) and *Bmp7* signalling. Both *Gpc3* and *Bmp7* were upregulated in $Wt1^{R394W/+}$ podocytes (supplementary material, Table S1), with upregulation of *Bmp7* reported to be protective in multiple models of mesangial injury [42,43]. Between podocytes and PECs, *Cxcl12-Sdc4* signalling was enriched (Figure 3E) in $Wt1^{R394W/+}$ glomeruli, a pathway implicated in the inhibition of PEC recolonisation in the injured glomerulus [44].

As both GO and ligand-receptor analyses indicate disruption to podocyte-derived angiogenic signalling in the $Wt1^{R394W/+}$ glomerulus, we conducted tube formation assays with wild-type primary murine GECs (supplementary material, Figure S2C) exposed to medium conditioned by podocytes harvested from 4-week-old $Wt1^{+/+}$ or $Wt1^{R394W/+}$ mice. Exposure of GECs to conditioned medium from $Wt1^{R394W/+}$ podocytes led to on average 30.6% significantly fewer endothelial loops ($p = 0.0200$; Figure 3G), along with significantly reduced total tube length (by 7.9%, $p = 0.0141$; Figure 3H), with each individual tube showing on average a 56.2% significantly longer length in $Wt1^{R394W/+}$ conditioned medium ($p = 0.0104$; Figure 3I). Overall, this led to GECs in $Wt1^{R394W/+}$ conditions forming fewer, wider loops, indicative of a less complex microvascular network (Figure 3J).

To evaluate the impact of this *in vivo*, we measured GEC coverage through disease progression in $Wt1^{+/+}$ and $Wt1^{R394W/+}$ mice. Unlike the onset of podocyte loss, which was present from 4 weeks, endothelial cell number ($CD31^+$ coverage/ tuft area) was maintained in 2-week-old ($Wt1^{+/+}$, 49.7 ± 3.7% and $Wt1^{R394W/+}$, 53.2. ± 2.8%) and 4-week-old ($Wt1^{+/+}$, 51.9 ± 1.3% and $Wt1^{R394W/+}$, 42.9 ± 4.0%) glomeruli, but showed a reduction of around 50% by 8 weeks of age ($Wt1^{+/+}$, 52.39 ± 4.0% versus $Wt1^{R394W/+}$, 22.0 ± 3.3%; $p < 0.0001$; Figure 4A,B). We also evaluated GEC coverage in human biopsies from WT1 glomerulopathies. Samples taken from four healthy paediatric donors (HPD1-4) showed an average $CD31^+$ endothelial coverage of 25.6 ± 4.0% (Figure 4C). Two of the three WT1 glomerulopathies analysed, including a WT1p.R366H (*WT1* c.*1097G > A*; p.Arg366His, 14.6 ± 3.8%) mutation, with thrombotic microangiopathy on histology [45] (Figure 4D,i) and the WT1p.R394W (17.55 ± 7.9%) mutation, with DMS on histology [46] (Figure 4D,ii), showed a significant reduction in GEC coverage compared with HPD1-4 ($p < 0.0001$). The third mutation, WT1p.H405R (*WT1 c.1214A > G*; p.His405Arg, 24.3 ± 3.8%), with areas of glomerular matrix expansion on histology [46] (Figure 4D,iii), showed no difference compared with HPD1-4 (Figure 4C–E).

Upregulated adrenomedullin supports endothelial angiogenesis in $Wt1^{R394W/+}$ glomeruli

The enrichment of adrenomedullin signalling between podocytes and GECs in $Wt1^{R394W/+}$ glomeruli (Figure 3D) led us to further investigate its role in the context of WT1 glomerulopathy. *Adm* is predominantly expressed in podocytes (Figure 5A) and its receptors in GECs (Figure 5B–D). Differential expression analyses demonstrated a significant upregulation ($log_2FC = 0.66$; Figure 5E and supplementary material, Table S1) of *Adm* in $Wt1^{R394W/+}$ podocytes. We next quantified circulating levels of pro-adrenomedullin (pro-AM), the precursor peptide for adrenomedullin, in plasma from $Wt1^{+/+}$ and $Wt1^{R394W/+}$ mice and found significantly elevated levels in 4-week-old $Wt1^{R394W/+}$ mice (log_{10} pro-AM 1.95 ± 0.23 pg/ml) compared with $Wt1^{+/+}$ (log_{10} pro-AM 1.55 ± 0.34 pg/ml; $p = 0.0081$), but no difference at 8 weeks of age (Figure 5F). To explore the role of podocyte *Adm* upregulation in the context of the anti-angiogenic environment found in *Wt1* glomerular disease (Figures 2H,I and 3D), we quantified secreted levels of pro-AM in the $Wt1^{R394W/+}$ podocyte conditioned medium used in tube formation assays and found a significant positive correlation with the number of loops ($p = 0.019$; Figure 5G) of cultured GECs. Together this suggests that despite the overall dampening of vascular signalling, adrenomedullin increases in early $Wt1^{R394W/+}$ disease, adopting a pro-angiogenic role in the glomerulus.

Subsequently, we repeated tube formation assays with $Wt1^{R394W/+}$ podocyte conditioned media with the addition of 200 nM of exogenous adrenomedullin. This supplementation resulted in the cultured GECs showing increased loop count (an average increase of 157.6%; $p = 0.0003$ versus $Wt1^{R394W/+}$ conditioned

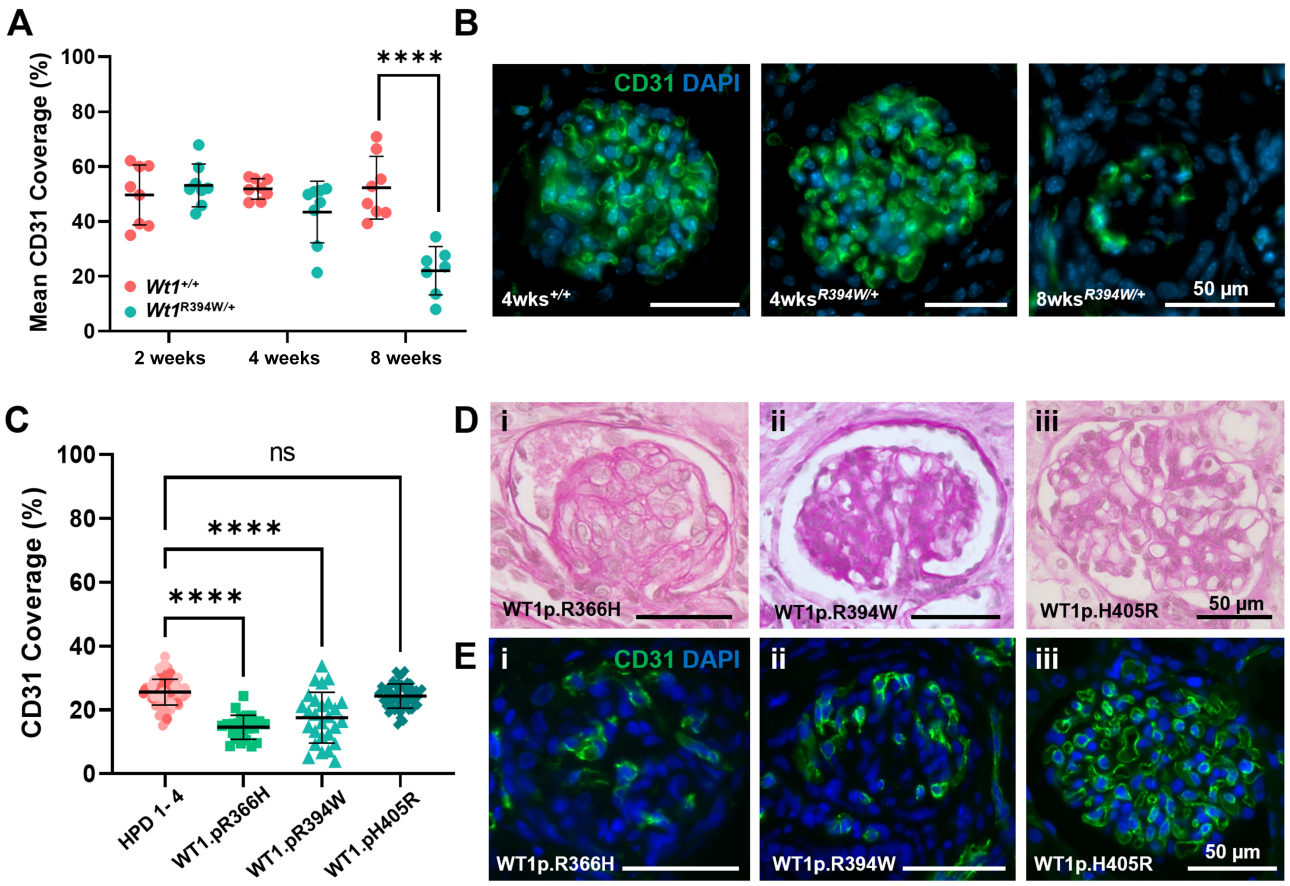

Figure 4. Glomerular endothelial loss in WT1 glomerulopathy in mouse and human tissues. (A) Endothelial cell ($CD31^+$) coverage/glomerular tuft area in murine glomeruli at 2 (*t*-test; $p = 0.4733$; $n = 8$ mice per group), 4 (*t*-test; $p = 0.0624$; $n = 8$ mice per group) and 8 weeks of age shows a significant decline in $CD31^+$ coverage by 8 weeks of age (*t*-test; $p < 0.0001$, $n = 8$ mice per group). (B) Representative images of $CD31^+$ coverage in the glomerular tuft in $Wt1^{+/+}$ and $Wt1^{R394W/+}$ mice at 4 weeks of age with similar endothelial coverage and $Wt1^{R394W/+}$ at 8 weeks of age when a significant loss in endothelial coverage is observed; scale bars: 50 µm. (C) Endothelial cell ($CD31^+$) coverage/glomerular tuft area in human glomeruli from biopsies taken from four healthy paediatric donors (pooled and indicated in gradient colours: HPD1, 22 glomeruli; HPD2, 42 glomeruli; HPD3, 20 glomeruli; and HPD4, 11 glomeruli) and three WT1 glomerulopathy donors, of which WT1.pR336H (one-way ANOVA, $p < 0.0001$, 25 glomeruli) and WT1.pR394W (one-way ANOVA, $p < 0.0001$, 27 glomeruli) showed a significant reduction of $CD31^+$ coverage, whereas WT1.pH405R (one-way ANOVA, $p = 0.3988$, 55 glomeruli) showed no significant difference in $CD31^+$ glomerular coverage compared with HPD1-4. (D, E) Representative glomerular histology of three WT1 glomerulopathy donors WT1.pR336H, WT1.pR394W and WT1.pH405R. (E) Representative images of $CD31^+$ coverage in the glomerular tuft of WT1 glomerulopathies, of which a significant loss in endothelial coverage is observed in WT1.pR336H and WT1.pR394W, but not in WT1.pH405R glomeruli when compared with HPD1–4; scale bars: 50 µm.

medium without supplementation; Figure 5H), alongside increased total tube length (by an average of 37.8%; $p < 0.0001$; Figure 5I) but with a reduction in the average length of each tube (by 53.0%; $p = 0.025$; Figure 5J), resulting in a denser, more complex endothelial network (Figure 5K). Together this suggests that *Adm* upregulation offers a protective response in $Wt1^{R394W/+}$ podocytes; however, at native expression levels, this upregulation is insufficient to combat the wider loss of other vascular factors.

Adrenomedullin upregulation is part of a common signature of podocyte injury across murine and human glomerulopathies

To explore the extent to which adrenomedullin upregulation is a common feature of podocyte injury across murine and human glomerulopathies, we conducted an integrated comparison of $Wt1^{R394W/+}$ glomeruli with three other murine scRNA-seq datasets [8]: (1) the nephrotoxic nephritis model (supplementary material, Figure S3A) of adult autoimmune glomerulonephritis; (2) a leptin-deficiency (BTBR $Lep^{ob/ob}$) model of adult DN (supplementary material, Figure S3B); and (3) a CD2AP-null ($Cd2ap^{-/-}$) model of congenital FSGS, which also results in compromised immune function due to the role of CD2AP in T-cell adhesion [47] (supplementary material, Figure S3C). Akin to our $Wt1^{R394W/+}$ dataset, scRNA-seq data from these models were taken during early disease, at the onset of proteinuria, but prior to pathological glomerular changes [8]. Podocyte DEGs were computed for each model and compared across all four pathologies (Figure 6A,B). This approach identified upregulation of *Adm* across all four mouse models as part of a common signature of 23 upregulated and five downregulated podocyte genes (Figure 6C); with 47 upregulated and 17 downregulated

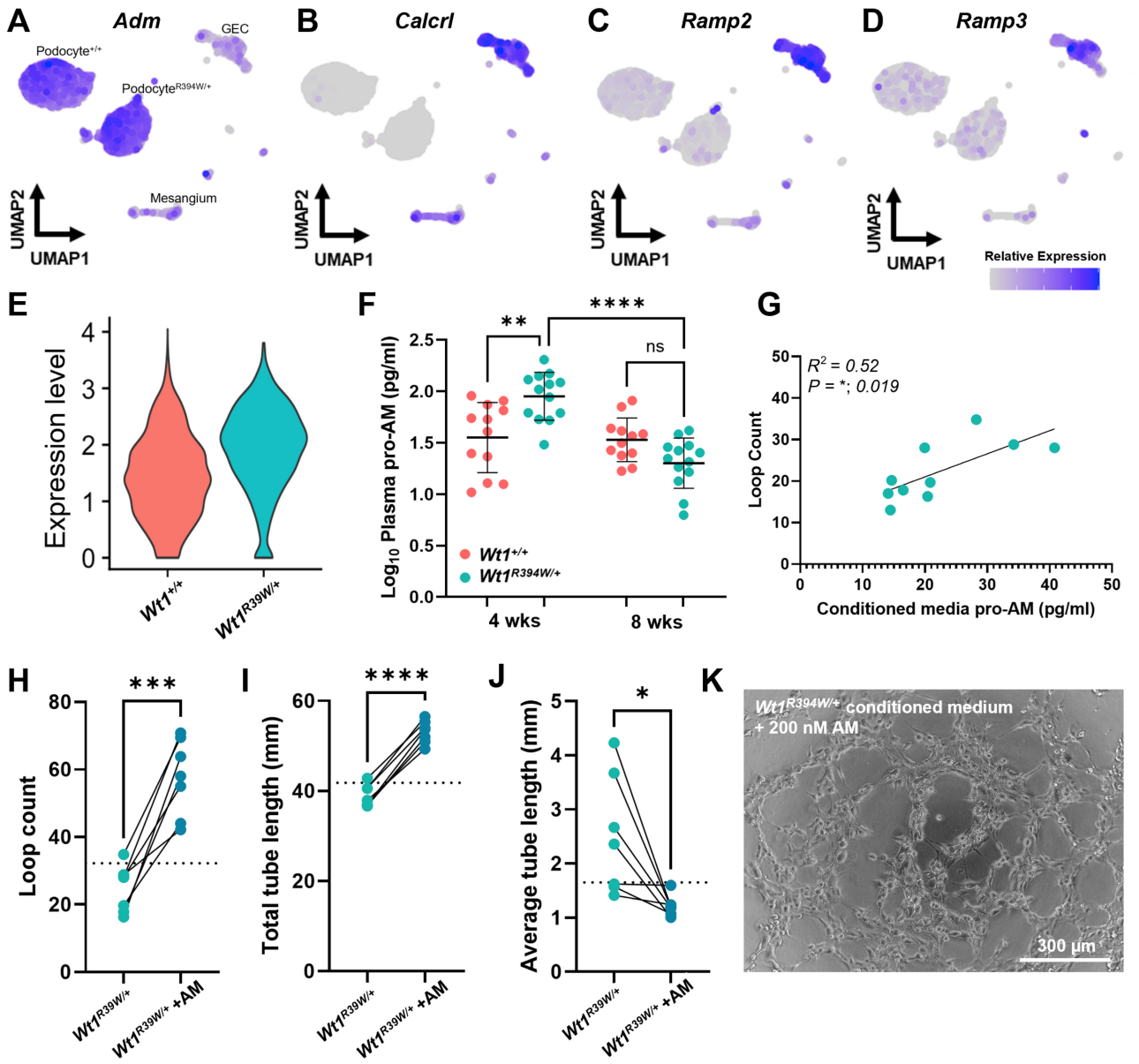

Figure 5. Adrenomedullin is upregulated in early disease in $Wt1^{R394W/+}$ mice and acts as a pro-angiogenic factor secreted by podocytes. Featureplots showing UMAP expression localisation of (A) *Adm* predominantly in podocytes and its receptors, (B) *Calcrl*, (C) *Ramp2* and (D) *Ramp3* in glomerular endothelial cells (GECs). (E) Violin plot of *Adm*, significantly upregulated in $Wt1^{R394W/+}$ podocytes [$\log_2$ fold change (FC) = 0.66]. (F) Plasma pro-adrenomedullin (pro-AM) levels are elevated in $Wt1^{R394W/+}$ mice (turquoise) compared with $Wt1^{+/+}$ littermates (pink) at 4 weeks of age (two-way ANOVA, $p = 0.0081$, $n = 12$ mice per group), an increase which is lost in $Wt1^{R394W/+}$ mice by 8 weeks of age (two-way ANOVA, $p < 0.0001$, $n = 12$ mice per group); lines represent mean ± SD. (G) Secreted levels of pro-AM in $Wt1^{R394W/+}$ podocyte conditioned medium positively correlate with loop count in cultured GECs (line fit by simple linear regression, two-tailed correlation analyses, $p = 0.019$). (H–J) Tube formation in murine GECs cultured in media conditioned by primary podocytes isolated from $Wt1^{R394W/+}$ mice at 4 weeks of age with and without the addition of adrenomedullin (AM; 200 nM) results in (H) more loops (paired *t*-test; $p = 0.0002$, $n = 7$ mice per group), (I) increased total tube length (paired *t*-test; $p < 0.0001$, $n = 7$ mice per group), (J) decreased average individual length (paired *t*-test; $p = 0.0165$, $n = 7$ mice per group); dashed line represents the average of the $Wt1^{+/+}$ conditioned media conditions. (K) Representative image of GEC tube formation in $Wt1^{R394W/+}$ podocyte conditioned medium with 200 nM AM.

genes in three or more of the four datasets (supplementary material, Table S2).

To explore the relevance of these conserved murine genes to human disease, we used Nephroseq to analyse human glomerular microarray datasets. These included variants of FSGS [48,49]; minimal change disease (MCD) [48,49]; three immune-mediated glomerulopathies, IgA nephropathy (IgAN) [48,50], membranous nephropathy (MN) [48] and lupus nephritis (LN) [48,51,52]; and DN [48,53]. Thirteen of the 28 (46.43%) transcripts differentially expressed across murine models were altered in at least one human glomerulopathy dataset (Table 1). *ADM* was upregulated (supplementary material, Figure S4Ai–iii) in three human disease datasets, *LGALS1* (supplementary material, Figure S4Bi–v), *CXCL1* (supplementary material, Figure S4Ci-–v)

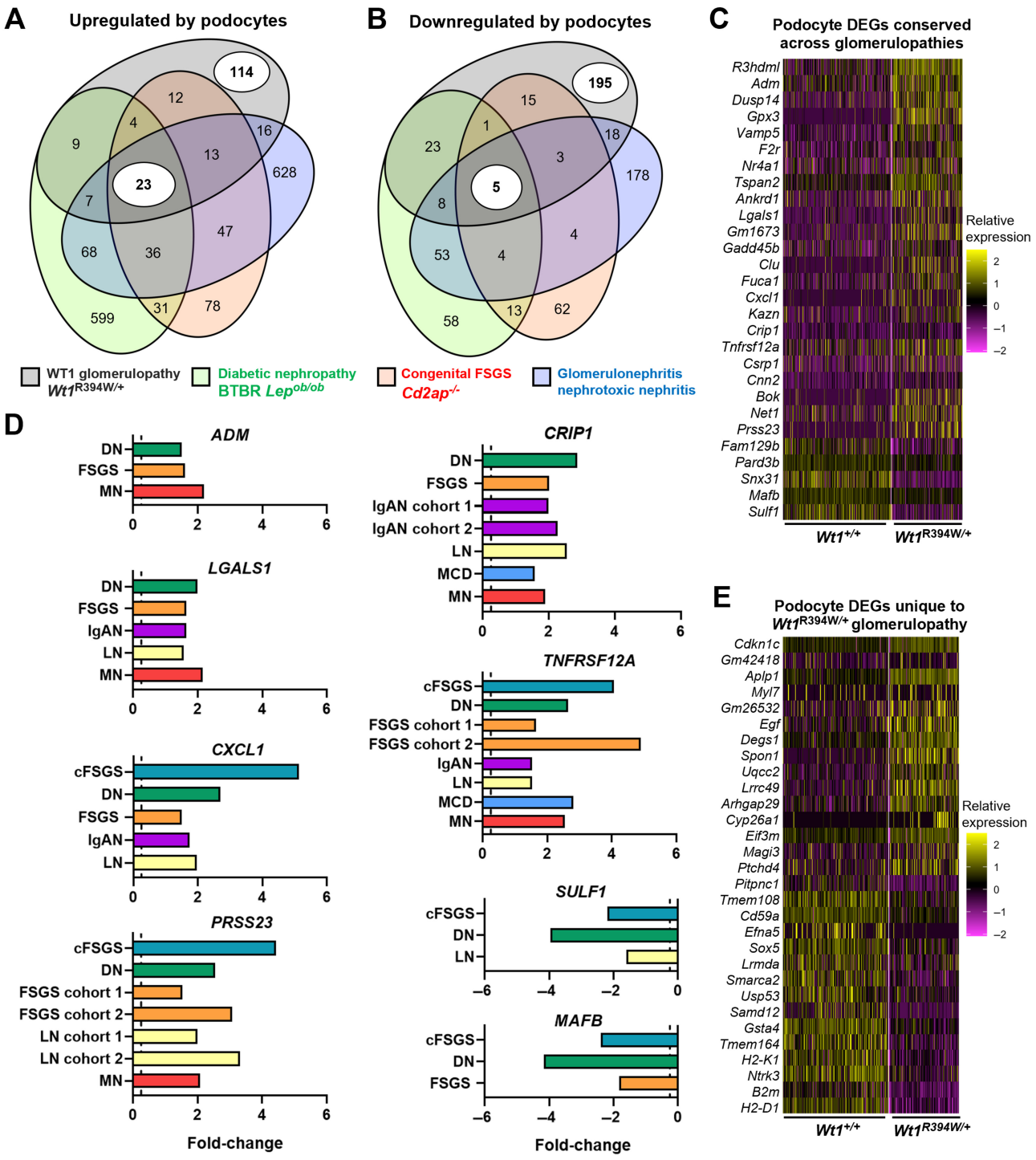

Figure 6. Damaged podocytes share a common signature in both murine and human glomerulopathies in children and adults, but *Wt1*$^{R394W/+}$ glomerulopathy has a specific transcriptional profile. (A) Venn diagram of upregulated differentially expressed genes (DEGs) in diseased podocytes across four murine models of early glomerular disease (*Wt1*$^{R394W/+}$, black; nephrotoxic nephritis, blue; *Lep*$^{ob/ob}$ diabetes, green; and *Cd2ap*$^{-/-}$, red), highlighting that the majority of *Wt1*$^{R394W/+}$ differentially expressed genes are unique, but 23 genes are common across all four glomerulopathies. (B) Venn diagram of downregulated podocyte differentially expressed genes across four murine models of early glomerular disease highlighting that the majority of *Wt1*$^{R394W/+}$ DEGs are unique, but five genes are common across all four glomerulopathies. (C) Heatmap of the 23 and 5 conserved podocyte genes in the *Wt1*$^{R394W/+}$ dataset that are up- or downregulated across four early disease murine glomerular models. (D) Bar charts of the fold-change increase or decrease of conserved genes in murine models similarly dysregulated in three or more human glomerular pathologies (microarray data, Nephroseq); HD, healthy donor; cFSGS, collapsing focal segmental glomerulosclerosis glomeruli; DN, diabetic nephropathy glomeruli; FSGS, focal segmental glomerulosclerosis glomeruli; IgAN, IgA nephropathy glomeruli; LN, lupus nephritis glomeruli; MCD, minimal change disease glomeruli; MN, membranous nephropathy glomeruli. (E) Heatmap of podocyte DEGs that are unique to *Wt1*$^{R394W/+}$ glomerulopathy and were not present in nephrotoxic nephritis, *Lep*$^{ob/ob}$ diabetes, or *Cd2ap*$^{-/-}$ models.

Table 1. Podocyte genes dysregulated in *Wt1*$^{R394W/+}$, nephrotoxic nephritis, *Lep*$^{ob/ob}$ diabetes and *Cd2ap*$^{-/-}$ murine scRNA-seq datasets, with associated changes in human glomerulopathies. All 23 upregulated and five downregulated podocyte genes found in four murine early disease datasets (*Wt1*$^{R394W/+}$, nephrotoxic nephritis, *Lep*$^{ob/ob}$ diabetes and *Cd2ap*$^{-/-}$) and their corresponding occurrence in human glomerular pathologies (Nephroseq).

Gene upregulated in four murine podocyte datasets	Gene; gene function	Upregulated in human datasets
R3hdml	R3H domain containing like; putative serine protease inhibitor	-
Adm	Adrenomedullin; vasodilation, hormone secretion, promotion of angiogenesis	DN, FSGS, MN
Dusp14	Dual specificity phosphatase 14; dephosphorylates tyrosine and serine/threonine	-
Gpx3	Glutathione peroxidase 3; protects against oxidative stress	-
Vamp5	Vesicle associated membrane protein 5; docking/fusion of vesicles and cell membranes	-
F2r (*Par1*)	Coagulation factor II Thrombin receptor; regulation of thrombotic response	-
Nr4a1 (*Nur77*)	Nuclear receptor-related factor 1; orphan nuclear receptor.	-
Tspan2	Tetraspanin 2; cell surface protein involved in signal transduction events	MG
Ankrd1 (*Carp*)	Ankyrin repeat domain 1; putative transcription factor	-
Lgals1	Galectin 1; modulates cell–cell and cell–matrix interactions, component of slit-diaphragm	DN, FSGS, IgAN, LN, MN
Gm1673 (*C4orf48*)	Neuropeptide-like protein C4orf48; unknown	cFSGS
Gadd45b	Growth arrest and DNA damage inducible beta; stress response gene	-
Clu	Clusterin; extracellular chaperone	DN
Fuca1	Alpha-L-fucosidase 1; lysosomal enzyme, degradation of fucose-glycoproteins/lipids	-
Cxcl1	C-X-C motif chemokine ligand 1; inflammatory chemokine	cFSGS, DN, FSGS, IgAN, LN
Kazn (*Kaz*)	Kazrin; desmosome assembly, cell adhesion, cytoskeletal organisation	cFSGS
Crip1	Cysteine rich protein 1; putative function as an intracellular zinc transport protein	DN, FSGS, IgAN, LN, MCD, MN
Tnfrsf12a (*Fn14*)	Tumor necrosis factor receptor superfamily member 12A; positive regulation of apoptosis	cFSGS, DN, FSGS, IgAN, LN, MCD, MN
Csrp1	Cysteine and glycine rich protein 1; putative role in development and cellular differentiation	-
Cnn2	Calponin 2; putative function in the structural organisation of actin filaments	-
Bok	BCL2 family apoptosis regulator BOK; a proapoptotic member of the BCL2 family	-
Net1	Neuroepithelial cell transforming 1; guanine nucleotide exchange factor for RhoA GTPase	LN
Prss23	Serine protease 23; trypsin family of serine proteases	cFSGS, DN, FSGS, LN, MN
Gene downregulated in four murine podocyte datasets	**Gene; gene function**	**Downregulated in human datasets**
Sulf1	Sulfatase 1; enzyme that removes 6-O-sulphate from proteoglycan heparan sulfate chains	cFSGS, DN, LN
Snx31	Sorting nexin 31; putative role in intracellular protein transport	-
Pard3b	Par-3 family cell polarity regulator beta; putative role in cell division and cell polarization	-
Mafb	MAF BZIP transcription factor B; transcription factor, required for podocyte differentiation	cFSGS, DN, FSGS
Fam129b (*Niban2*)	Niban apoptosis regulator 2; transcriptional coactivator, putative anti-apoptosis role	-

cFSGS, collapsing focal segmental glomerulosclerosis glomeruli; DN, diabetic nephropathy glomeruli; FSGS, focal segmental glomerulosclerosis glomeruli; HD, healthy donor; IgAN, IgA nephropathy glomeruli; LN, lupus nephritis glomeruli; MCD, minimal change disease glomeruli; MN, membranous nephropathy glomeruli.

and *PRSS23* (supplementary material, Figure S4Di–vii) transcripts were significantly elevated in five, *CRIP1* (supplementary material, Figure S4Ei–vi) upregulated in six and *TNFRSF12A* (supplementary material, Figure S4Fi–viii) increased in seven glomerular disease datasets (Figure 6D). *SULF1* (supplementary material, Figure S4Gi–iii) and *MAFB* (supplementary material, Figure S4Hi–iii) were downregulated in three human disease datasets.

WT1 glomerulopathy has a unique transcriptional signature

By performing comparative analyses across murine podocyte scRNA-seq datasets, we also revealed disease-specific transcriptional changes (Figure 6A,B). Focusing on WT1 glomerulopathy, the 114 upregulated (57.3% of the total upregulated) and 195 downregulated (72.8% of the total downregulated) genes unique to *Wt1*$^{R394W/+}$ disease point towards its distinct aetiology (supplementary material, Table S2); the top 30 unique genes (by $\log_2$FC) are shown in Figure 6E.

With this in mind, we explored a key aetiological hallmark of WT1 glomerulopathy and other congenital glomerular diseases, their resistance to glucocorticoids and second-line immunosuppressive therapies [1,2,12]. To do so, we interrogated the list of unique DEGs from each of the four early disease murine podocyte datasets, identifying those classified in the broadest immunological GO term (GO:0002376 – *immune system process*). The unique podocyte DEGs from nephrotoxic nephritis, DN and *Cd2ap*$^{-/-}$ models all showed an overall upregulation of genes involved in '*immune system processes*'. In contrast, *Wt1*$^{R394W/+}$ was the only model in

which a downregulation of this GO term dominated (supplementary material, Table S3); an observation fitting with the lack of monocyte influx noted in $Wt1^{R394W/+}$ glomeruli (Figure 2G and supplementary material, Figure S1G). This suppression in $Wt1^{R394W/+}$ podocytes is unlikely to reflect direct WT1 mis-regulation, as only two of the 14 immune-related genes were predicted to contain a WT1 regulatory element.

Discussion

Our results constitute the first scRNA-seq glomerular dataset of a childhood glomerulopathy, which models a clinically relevant point mutation observed in patients. Podocytes are the most altered glomerular cell-type in early $Wt1^{R394W/+}$ pathology, consistent with the localisation of WT1 in the postnatal kidney and the predicted dominant-negative effect of mutant WT1 when binding DNA [54,55]. Our ligand-receptor analysis has highlighted alterations to cell–cell communication in the $Wt1^{R394W/+}$ glomerulus during the early stages of disease, with a pronounced role for disrupted angiogenic signalling and a significant reduction of *Vegfa* and *Nrp1*. We subsequently showed GEC loss in the $Wt1^{R394W/+}$ mouse during later disease. Previous temporal characterisation of disease progression found no overt changes in kidney histology in newborn or 3-week-old $Wt1^{R394W/+}$ animals [11]. However, the pre-natal phenotype of $Wt1^{R394W/+}$ mice should be examined in finer detail, using methods such as three-dimensional imaging [56], as the human pathology of WT1 glomerulopathies manifests early after birth and thus is likely to have an initial insult during nephrogenesis. This could also be examined using human $Wt1^{R394W/+}$ kidney organoids, but at present kidney organoid culture does not facilitate the differentiation of vascularised glomeruli with capillary loops and *in vivo* vascularisation through murine implantation is required [57]. The $Wt1^{R362X/+}$ truncation mouse model of DDS also displays glomeruli with fewer capillary loops and lower expression of CD31 [58]. However, this was assessed at E18.5, due to postnatal lethality. Postnatal damage to GECs was also apparent in paediatric biopsies from two WT1 glomerulopathies, notably that of the heterozygous p.R394W point mutation [46] and a p.R366H mutation [45], but not of a p.H405R mutation [46,59]. This highlights mutation-associated variation in pathology, perhaps in accordance with the severity of abnormal glomerular development [58] or postnatal damage.

We also found that the vascular peptide adrenomedullin was upregulated in $Wt1^{R394W/+}$ podocytes (*Adm*) and plasma (Pro-AM). Adrenomedullin adopts multiple roles within the kidney; from vasodilatory and diuretic functions, to the regulation of cellular proliferation and inflammation [37]. Adrenomedullin upregulation appears to offer a pro-angiogenic protective response in the dampened angiogenic environment of the $Wt1^{R394W/+}$ glomerulus in early disease. However, this response is an ineffective one, in the context of the broader loss of other vascular signalling molecules, which results in endothelial cell loss in advancing disease. Indeed, the upregulation of *ADM* in progressive human pathologies raises the same point of incomplete protection. Thus, the extent to which the native upregulation of this molecule impacts disease progression is an area of future investigation. However further administration of adrenomedullin was able to rescue impaired loop formation, supporting microvasculature complexity in GECs tube formation assays. Together this suggests that vascular-focused therapies, which have been used in adult pre-clinical models of kidney disease [60,61], may offer an early, targeted approach to alleviate the disruption in podocyte vascular signalling in certain WT1 glomerulopathies. Among these, adrenomedullin, as a natively upregulated angiogenic molecule that shows complete rescue *in vitro* with further administration, warrants further investigation.

By integrating our $Wt1^{R394W/+}$ dataset with other murine models and human glomerular diseases, we identified a signature of molecules that define podocyte injury and offer promise for future treatment approaches. The eight identified genes span a variety of functions. *ADM* was upregulated in human glomeruli from FSGS, MN and DN, with others describing elevated plasma levels in patients with non-diabetic CKD [62,63]. As mentioned, this supports broader therapeutic implications for *ADM*, as demonstrated in multiple experimental models of podocyte injury [39–41]. However, this efficacy is pathology dependent and may not always be advantageous, as reported in DN, where elevated levels are linked to increased angiogenesis, a pathological hallmark of the early diabetic glomerulus [64,65]. *SULF1* (sulfatase-1; supplementary material, Table S1) is a modulator of growth factor signalling in the GBM and is a direct target of WT1 [22]. The global $Sulf1^{-/-}$; $Sulf2^{-/-}$ mouse displays proteinuria, glomerulosclerosis and a reduced distribution of VEGFA in the GBM [66,67], supporting a role for *SULF1* beyond that of WT1 glomerulopathy alone. Galectin-1 is a component of the slit-diaphragm, and its increased glomerular expression is a feature of childhood DMS and FSGS [68], as well as adult DN [69]. *MAFB* encodes a transcription factor required for maintenance of podocyte differentiation and is decreased in podocytes from patients with FSGS [70]. In contrast, *CRIP1* expression is yet to be described in podocytes but is defined as a marker of juxtaglomerular renin cells [71]. Similarly, serine protease 23 (*PRSS23*) has received little attention in the context of glomerular disease, but it is upregulated in human FSGS glomeruli [72] and in podocytes and mesangial cells from a $Cd2ap^{+/-}$; $Fyn^{-/-}$ mouse model of FSGS [73]. The final two transcripts *CXCL1* and *TNFRSF12A*, upregulated in five and seven human datasets respectively, both encode immune factors. CXCL1 is a chemokine implicated in glomerulonephritis, regulating infiltration of neutrophils into the

glomerulus [74] while TNFRSF12A promotes inflammation and fibrosis in LN [75] and crescent formation in IgAN [76]. Our findings show upregulation of *CXCL1* and *TNFRSF12A* in both glomerulonephritis and nephrotic diseases with a non-immune origin.

Finally, we highlight a critical feature of WT1 glomerulopathy, where a decrease in immune-related genes defines early pathology and offers a potential explanation for the suboptimal efficacy of immunosuppressive drugs in clinical practice. This was recently evaluated for calcineurin inhibitors, immunosuppressive medications with emerging efficacy in genetic SRNS, which showed no remission response in patients with *WT1 v*ariants, compared with 2.2% and 15.4% in *NPHS2* and *NPHS1* variant cohorts, respectively [77]. Together this necessitates examination of other genetic variants of congenital glomerular disease (which, unlike CD2AP, have no immunological function) to ascertain if this immunological feature is a unique hallmark of WT1 disease. Our findings point towards the alternative approach of vascular based therapies, which may modulate disrupted podocyte cell signalling and the associated loss of GECs that occurs concurrently with decline in kidney function.

Acknowledgements

The authors would like to thank Dr Karin Straathof for her use of the 10× Chromium Controller and Dr Ayad Eddaoudi and the UCL Flow Cytometry Core Facility. This work was supported by a Wellcome Trust Investigator Award (220895/Z/20/Z, to DAL), a National Institute for Health Research (NIHR) Biomedical Research Centre at Great Ormond Street Hospital for Children NHS Foundation Trust and University College London Catalyst Fellowship (to JCC) and a Kidney Research UK (KRUK) Intermediate Fellowship (INT_004_20210727 to JCC), a KRUK Research Project Grant (Paed_RP_011_20170929, to AMW, DAL and JCC), a LifeArc/Great Ormond Street Children's Charity research project grant (VS0322, to DAL, JCC and AMW), an MRC project grant (MR/T016809/1 to ASW), a BHF grant (PG/18/31/33759 to DOB and AVB) and Nottingham University Cancer Research Priority Area funding and PhD studentships from Diabetes UK (17/0005733, to GP, DAL) and the London Interdisciplinary Biosciences BBSRC funded Doctoral Training Partnerships (to SM, DAL). DJJ is supported by the UCL MB/PhD programme, a Child Health Research PhD studentship, a Rosetrees Trust PhD Plus award (PhD2020\100012) and a Foulkes Foundation Fellowship for postdoctoral research.

Author contributions statement

JCC, DAL and AMW conceived and designed the project. AVB and DOB rederived mouse line. JCC conducted characterisation of the mouse line, optimised single-cell preparation, performed dynabead perfusions with MKJ. and conducted the scRNA-seq protocol, with 10× machine support from AP. JCC isolated primary podocytes for transcript analysis and was responsible for podocyte culture, RT-qPCR analysis and tube formation assays. JCC conducted gene searching in Nephroseq. DJJ, GP and ASM performed all scRNA-seq bioinformatical analyses, in particular DJJ performed cell annotation, differential expression analyses, gene ontology and intercellular communication analyses and GP conducted WT1 motif analyses. JCC manually curated cell–cell interaction outputs. SM and MB performed immunostaining, imaging and cell-counting analysis on murine tissue with support from WJM. RAS, AL, OB and KPJ provided histology support and human tissue samples. ASW supported data interpretation, JCC and DJJ collated and presented the figures and JCC, DJJ and DAL wrote the manuscript with assistance from ASW and PJW.

Data availability statement

Primary sequencing data reported in this paper are available on NCBI Sequence Read Archive (SRA PRJNA928337). Processed data for scRNA-seq experiments are available on Zenodo at DOI: 10.5281/zenodo.7565867.

The codes generated during this study are available at Github repository https://github.com/daniyal-jafree1995/collaborations. All other unique reagents used in this study are available from the corresponding author on reasonable request.

References

1. Cheong HI. Genetic tests in children with steroid-resistant nephrotic syndrome. *Kidney Res Clin Pract* 2020; **39:** 7–16.
2. Ranganathan S. Pathology of podocytopathies causing nephrotic syndrome in children. *Front Pediatr* 2016; **4:** 32.
3. Wang ZY, Qiu QQ, Deuel TF. The Wilms' tumor gene product WT1 activates or suppresses transcription through separate functional domains. *J Biol Chem* 1993; **268:** 9172–9175.
4. Lefebvre J, Clarkson M, Massa F, *et al*. Alternatively spliced isoforms of WT1 control podocyte-specific gene expression. *Kidney Int* 2015; **88:** 321–331.
5. Kann M, Ettou S, Jung YL, *et al*. Genome-wide analysis of Wilms' tumor 1-controlled gene expression in podocytes reveals key regulatory mechanisms. *J Am Soc Nephrol* 2015; **26:** 2097–2104.
6. Hartwig S, Ho J, Pandey P, *et al*. Genomic characterization of Wilms' tumor suppressor 1 targets in nephron progenitor cells during kidney development. *Development* 2010; **137:** 1189–1203.
7. He B, Chen P, Zambrano S, *et al*. Single-cell RNA sequencing reveals the mesangial identity and species diversity of glomerular cell transcriptomes. *Nat Commun* 2021; **12:** 2141.
8. Chung JJ, Goldstein L, Chen YJJ, *et al*. Single-cell transcriptome profiling of the kidney glomerulus identifies key cell types and reactions to injury. *J Am Soc Nephrol* 2020; **31:** 2341–2354.
9. Clark AR, Marshall J, Zhou Y, *et al*. Single-cell transcriptomics reveal disrupted kidney filter cell-cell interactions after early and selective podocyte injury. *Am J Pathol* 2022; **192:** 281–294.

10. Zambrano S, He L, Kano T, *et al*. Molecular insights into the early stage of glomerular injury in IgA nephropathy using single-cell RNA sequencing. *Kidney Int* 2022; **101:** 752–765.
11. Gao F, Maiti S, Sun G, *et al*. The Wt1+/R394W mouse displays glomerulosclerosis and early-onset renal failure characteristic of human Denys-Drash syndrome. *Mol Cell Biol* 2004; **24:** 9899–9910.
12. Lipska BS, Ranchin B, Iatropoulos P, *et al*. Genotype-phenotype associations in WT1 glomerulopathy. *Kidney Int* 2014; **85:** 1169–1178.
13. Little M, Wells C. A clinical overview of WT1 gene mutations. *Hum Mutat* 1997; **9:** 209–225.
14. Korin B, Chung JJ, Avraham S, *et al*. Preparation of single-cell suspensions of mouse glomeruli for high-throughput analysis. *Nat Protoc* 2021; **16:** 4068–4083.
15. Dumas SJ, Meta E, Borri M, *et al*. Phenotypic diversity and metabolic specialization of renal endothelial cells. *Nat Rev Nephrol* 2021; **17:** 441–464.
16. Zimmerman KA, Bentley MR, Lever JM, *et al*. Single-cell RNA sequencing identifies candidate renal resident macrophage gene expression signatures across species. *J Am Soc Nephrol* 2019; **30:** 767–781.
17. Karaiskos N, Rahmatollahi M, Boltengagen A, *et al*. A single-cell transcriptome atlas of the mouse glomerulus. *J Am Soc Nephrol* 2018; **29:** 2060–2068.
18. Raredon MSB, Yang J, Kothapalli N, *et al*. Comprehensive visualization of cell–cell interactions in single-cell and spatial transcriptomics with NICHES. *Bioinformatics* 2023; **39:** btac775.
19. Schindelin J, Arganda-Carreras I, Frise E, *et al*. Fiji: an open-source platform for biological-image analysis. *Nat Methods* 2012; **9:** 676–682.
20. Vasilopoulou E, Kolatsi-Joannou M, Lindenmeyer MT, *et al*. Loss of endogenous thymosin β4 accelerates glomerular disease. *Kidney Int* 2016; **90:** 1056–1070.
21. Gearing LJ, Cumming HE, Chapman R, *et al*. CiiiDER: a tool for predicting and analysing transcription factor binding sites. *PLoS One* 2019; **14:** e0215495.
22. Ratelade J, Arrondel C, Hamard G, *et al*. A murine model of Denys-Drash syndrome reveals novel transcriptional targets of WT1 in podocytes. *Hum Mol Genet* 2010; **19:** 1–15.
23. Ishikawa T, Takemoto M, Akimoto Y, *et al*. A novel podocyte protein, R3h domain containing-like, inhibits TGF-β-induced p38 MAPK and regulates the structure of podocytes and glomerular basement membrane. *J Mol Med (Berl)* 2021; **99:** 859–876.
24. Fu J, Shinjo T, Li Q, *et al*. Regeneration of glomerular metabolism and function by podocyte pyruvate kinase M2 in diabetic nephropathy. *JCI Insight* 2022; **7:** e155260.
25. Henique C, Bollée G, Loyer X, *et al*. Genetic and pharmacological inhibition of microRNA-92a maintains podocyte cell cycle quiescence and limits crescentic glomerulonephritis. *Nat Commun* 2017; **8:** 1829.
26. Hiromura K, Haseley LA, Zhang P, *et al*. Podocyte expression of the CDK-inhibitor p57 during development and disease. *Kidney Int* 2001; **60:** 2235–2246.
27. Barisoni L, Mokrzycki M, Sablay L, *et al*. Podocyte cell cycle regulation and proliferation in collapsing glomerulopathies. *Kidney Int* 2000; **58:** 137–143.
28. Shankland SJ, Eitner F, Hudkins KL, *et al*. Differential expression of cyclin-dependent kinase inhibitors in human glomerular disease: role in podocyte proliferation and maturation. *Kidney Int* 2000; **58:** 674–683.
29. Randles MJ, Woolf AS, Huang JL, *et al*. Genetic background is a key determinant of glomerular extracellular matrix composition and organization. *J Am Soc Nephrol* 2015; **26:** 3021–3034.
30. Roberts-Pilgrim AM, Makareeva E, Myles MH, *et al*. Deficient degradation of homotrimeric type I collagen, α1(I)3 glomerulopathy in oim mice. *Mol Genet Metab* 2011; **104:** 373–382.
31. Connell LE, Helfman DM. Myosin light chain kinase plays a role in the regulation of epithelial cell survival. *J Cell Sci* 2006; **119:** 2269–2281.
32. Chen Z, Zhang T, Mao K, *et al*. A single-cell survey of the human glomerulonephritis. *J Cell Mol Med* 2021; **25:** 4684–4695.
33. Foster MC, Inker LA, Hsu CY, *et al*. Filtration markers as predictors of ESRD and mortality in southwestern American Indians with type 2 diabetes. *Am J Kidney Dis* 2015; **66:** 75–83.
34. Gorski M, van der Most PJ, Teumer A, *et al*. 1000 genomes-based meta-analysis identifies 10 novel loci for kidney function. *Sci Rep* 2017; **7:** 45040.
35. McCarty G, Awad O, Loeb DM. WT1 protein directly regulates expression of vascular endothelial growth factor and is a mediator of tumor response to hypoxia. *J Biol Chem* 2011; **286:** 43634–43643.
36. Koch S, van Meeteren LA, Morin E, *et al*. NRP1 presented in trans to the endothelium arrests VEGFR2 endocytosis, preventing angiogenic signaling and tumor initiation. *Dev Cell* 2014; **28:** 633–646.
37. Nishikimi T. Adrenomedullin in the kidney-renal physiological and pathophysiological roles. *Curr Med Chem* 2007; **14:** 1689–1699.
38. Hellenthal KEM, Brabenec L, Wagner NM. Regulation and dysregulation of endothelial permeability during systemic, inflammation. *Cells* 2022; **11:** 1935.
39. Dong N, Meng L, Xue R, *et al*. Adrenomedullin ameliorates podocyte injury induced by puromycin aminonucleoside in vitro and in vivo through modulation of rho GTPases. *Int Urol Nephrol* 2017; **49:** 1489–1506.
40. Oba S, Hino M, Fujita T. Adrenomedullin protects against oxidative stress-induced podocyte injury as an endogenous antioxidant. *Nephrol Dial Transplant* 2008; **23:** 510–517.
41. Hino M, Nagase M, Kaname S, *et al*. Expression and regulation of adrenomedullin in renal glomerular podocytes. *Biochem Biophys Res Commun* 2005; **330:** 178–185.
42. Yeh CH, Chang CK, Cheng MF, *et al*. The antioxidative effect of bone morphogenetic protein-7 against high glucose-induced oxidative stress in mesangial cells. *Biochem Biophys Res Commun* 2009; **382:** 292–297.
43. Chan WL, Leung JC, Chan LY, *et al*. BMP-7 protects mesangial cells from injury by polymeric IgA. *Kidney Int* 2008; **74:** 1026–1039.
44. Romoli S, Angelotti ML, Antonelli G, *et al*. CXCL12 blockade preferentially regenerates lost podocytes in cortical nephrons by targeting an intrinsic podocyte-progenitor feedback mechanism. *Kidney Int* 2018; **94:** 1111–1126.
45. Berthaud R, Heidet L, Oualha M, *et al*. Atypical severe early-onset nephrotic syndrome: answers. *Pediatr Nephrol* 2022; **37:** 2637–2642.
46. Falcone MP, Pritchard-Jones K, Brok J, *et al*. Long-term kidney function in children with Wilms tumour and constitutional WT1 pathogenic variant. *Pediatr Nephrol* 2022; **37:** 821–832.
47. Shih NY, Li J, Karpitskii V, *et al*. Congenital nephrotic syndrome in mice lacking CD2-associated protein. *Science* 1999; **286:** 312–315.
48. Ju W, Greene CS, Eichinger F, *et al*. Defining cell-type specificity at the transcriptional level in human disease. *Genome Res* 2013; **23:** 1862–1873.
49. Hodgin JB, Borczuk AC, Nasr SH, *et al*. A molecular profile of focal segmental glomerulosclerosis from formalin-fixed, paraffin-embedded tissue. *Am J Clin Pathol* 2010; **177:** 1674–1686.
50. Reich HN, Tritchler D, Cattran DC, *et al*. A molecular signature of proteinuria in glomerulonephritis. *PLoS One* 2010; **5:** e13451.
51. Berthier CC, Bethunaickan R, Gonzalez-Rivera T, *et al*. Cross-species transcriptional network analysis defines shared inflammatory responses in murine and human lupus nephritis. *J Immunol* 2012; **189:** 988–1001.
52. Peterson KS, Huang JF, Zhu J, *et al*. Characterization of heterogeneity in the molecular pathogenesis of lupus nephritis from transcriptional profiles of laser-captured glomeruli. *J Clin Invest* 2004; **113:** 1722–1733.
53. Woroniecka KI, Park AS, Mohtat D, *et al*. Transcriptome analysis of human diabetic kidney disease. *Diabetes* 2011; **60:** 2354–2369.
54. Little MH, Williamson KA, Mannens M, *et al*. Evidence that WT1 mutations in Denys-Drash syndrome patients may act in a dominant-negative fashion. *Hum Mol Genet* 1993; **2:** 259–264.

55. Little M, Holmes G, Bickmore W, *et al*. DNA binding capacity of the WT1 protein is abolished by Denys-Drash syndrome WT1 point mutations. *Hum Mol Genet* 1995; **4:** 351–358.
56. Jafree DJ, Moulding D, Kolatsi-Joannou M, *et al*. Spatiotemporal dynamics and heterogeneity of renal lymphatics in mammalian development and cystic kidney disease. *Elife* 2019; **8:** e48183.
57. Bantounas I, Ranjzad P, Tengku F, *et al*. Generation of functioning nephrons by implanting human pluripotent stem cell-derived kidney progenitors. *Stem Cell Reports* 2018; **10:** 766–779.
58. Natoli TA, Liu J, Eremina V, *et al*. A mutant form of the Wilms' tumor suppressor gene WT1 observed in Denys-Drash syndrome interferes with glomerular capillary development. *J Am Soc Nephrol* 2002; **13:** 2058–2067.
59. Hu M, Craig J, Howard N, *et al*. A novel mutation of *WT1* exon 9 in a patient with Denys-Drash syndrome and pyloric stenosis. *Pediatr Nephrol* 2004; **19:** 1160–1163.
60. Gnudi L, Benedetti S, Woolf AS, *et al*. Vascular growth factors play critical roles in kidney glomeruli. *Clin Sci (Lond)* 2015; **129:** 1225–1236.
61. Long DA, Norman JT, Fine LG. Restoring the renal microvasculature to treat chronic kidney disease. *Nat Rev Nephrol* 2012; **8:** 244–250.
62. Dieplinger B, Mueller T, Kollerits B, *et al*. Pro-A-type natriuretic peptide and pro-adrenomedullin predict progression of chronic kidney disease: the MMKD study. *Kidney Int* 2009; **75:** 408–414.
63. Ishimitsu T, Nishikimi T, Saito Y, *et al*. Plasma levels of adrenomedullin, a newly identified hypotensive peptide, in patients with hypertension and renal failure. *J Clin Invest* 1994; **94:** 2158–2161.
64. El Eter EA, Al-Masri AA. Adrenomedullin mediates early phase angiogenesis induced diabetic nephropathy in STZ diabetic rats. *Eur Rev Med Pharmacol Sci* 2014; **18:** 3534–3543.
65. Nakagawa T, Kosugi T, Haneda M, *et al*. Abnormal angiogenesis in diabetic nephropathy. *Diabetes* 2009; **58:** 1471–1478.
66. Schumacher VA, Schlötzer-Schrehardt U, Karumanchi SA, *et al*. WT1-dependent sulfatase expression maintains the normal glomerular filtration barrier. *J Am Soc Nephrol* 2011; **22:** 1286–1296.
67. Takashima Y, Keino-Masu K, Yashiro H, *et al*. Heparan sulfate 6-O-endosulfatases, Sulf1 and Sulf2, regulate glomerular integrity by modulating growth factor signaling. *Am J Physiol Renal Physiol* 2016; **310:** F395–F408.
68. Ostalska-Nowicka D, Zachwieja J, Nowicki M, *et al*. Immunohistochemical detection of galectin-1 in renal biopsy specimens of children and its possible role in proteinuric glomerulopathies. *Histopathology* 2007; **51:** 468–476.
69. Liu Y, Long L, Yuan F, *et al*. High glucose-induced Galectin-1 in human podocytes implicates the involvement of Galectin-1 in diabetic nephropathy. *Cell Biol Int* 2015; **39:** 217–223.
70. Usui T, Morito N, Shawki HH, *et al*. Transcription factor MafB in podocytes protects against the development of focal segmental glomerulosclerosis. *Kidney Int* 2020; **98:** 391–403.
71. Brunskill EW, Sequeira-Lopez ML, Pentz ES, *et al*. Genes that confer the identity of the renin cell. *J Am Soc Nephrol* 2011; **22:** 2213–2225.
72. Bennett MR, Czech KA, Arend LJ, *et al*. Laser capture microdissection-microarray analysis of focal segmental glomerulosclerosis glomeruli. *Nephron Exp Nephrol* 2007; **107:** e30–e40.
73. Potter AS, Drake K, Brunskill EW, *et al*. A bigenic mouse model of FSGS reveals perturbed pathways in podocytes, mesangial cells and endothelial cells. *PLoS One* 2019; **14:** e0216261.
74. Chung AC, Lan HY. Chemokines in renal injury. *J Am Soc Nephrol* 2011; **22:** 802–809.
75. Michaelson JS, Wisniacki N, Burkly LC, *et al*. Role of TWEAK in lupus nephritis: a bench-to-bedside review. *J Autoimmun* 2012; **39:** 130–142.
76. Sasaki Y, Shimizu Y, Suzuki Y, *et al*. TWEAK/Fn14 system and crescent formation in IgA nephropathy. *BMC Nephrol* 2015; **16:** 27.
77. Malakasioti G, Iancu D, Milovanova A, *et al*. A multicenter retrospective study of calcineurin inhibitors in nephrotic syndrome secondary to podocyte gene variants. *Kidney Int* 2023; **103:** 962–972.
78. Zheng GX, Terry JM, Belgrader P, *et al*. Massively parallel digital transcriptional profiling of single cells. *Nat Commun* 2017; **8:** 14049.
79. Kim D, Paggi JM, Park C, *et al*. Graph-based genome alignment and genotyping with HISAT2 and HISAT-genotype. *Nat Biotechnol* 2019; **37:** 907–915.
80. Hao Y, Hao S, Andersen-Nissen E, *et al*. Integrated analysis of multimodal single-cell data. *Cell* 2021; **184:** 3573–3587.e29.
81. McGinnis CS, Murrow LM, Gartner ZJ. DoubletFinder: doublet detection in single-cell RNA sequencing data using artificial nearest neighbors. *Cell Syst* 2019; **8:** 329–337.e4.
82. Young MD, Behjati S. SoupX removes ambient RNA contamination from droplet-based single-cell RNA sequencing data. *Gigascience* 2020; **9:** giaa151.
83. Mi H, Muruganujan A, Huang X, *et al*. Protocol update for large-scale genome and gene function analysis with the PANTHER classification system (v.14.0). *Nat Protoc* 2019; **14:** 703–721.
84. Türei D, Korcsmáros T, Saez-Rodriguez J. OmniPath: guidelines and gateway for literature-curated signaling pathway resources. *Nat Methods* 2016; **13:** 966–967.
85. Szklarczyk D, Gable AL, Nastou KC, *et al*. The STRING database in 2021: customizable protein-protein networks, and functional characterization of user-uploaded gene/measurement sets. *Nucleic Acids Res* 2021; **49:** D605–D612.
86. Korsunsky I, Millard N, Fan J, *et al*. Fast, sensitive and accurate integration of single-cell data with harmony. *Nat Methods* 2019; **16:** 1289–1296.
87. Hernandez-Diaz I, Pan J, Ricciardi CA, *et al*. Overexpression of circulating soluble Nogo-B improves diabetic kidney disease by protecting the vasculature. *Diabetes* 2019; **68:** 1841–1852.

References 78–87 are cited only in supplementary materials

SUPPLEMENTARY MATERIAL ONLINE

Supplementary materials and methods

Figure S1. Supporting data for single-cell RNA seq analyses

Figure S2. Characterisation of primary cell lines

Figure S3. Isolation of podocytes from scRNA-seq data from additional murine models of glomerular disease for cross-disease comparison

Figure S4. Dysregulated genes shown by individual sample for each human glomerular pathology (source Nephroseq)

Table S1. Differentially expressed genes in glomerular cells in $Wt1^{R394W/+}$ mice

Table S2. Podocyte differentially expressed genes that are conserved across murine glomerular scRNA-seq datasets or unique to $Wt1^{R394W/+}$

Table S3. Podocyte differentially expressed genes classified in 'GO:0002376 – *immune system process*' across murine glomerular scRNA-seq datasets